Detection of Low Amplitude, In-Vivo Intrinsic Signals from an Optical Imager of Retinal Function.

Eduardo S. Barriga[1], Dan T'so[2], Marios Pattichis[1], Young Kwon[3], Randy Kardon[3], Michael Abramoff[3], and Peter Soliz[4]
[1] University of New Mexico, Albuquerque, NM, [2]SUNY Upstate University, Syracuse, NY,
[3]University of Iowa, Iowa City, IA, [4]VisionQuest Biomedical, Albuquerque, NM.

ABSTRACT

In the early stages of some retinal diseases, such as glaucoma, loss of retinal activity may be difficult to detect with today's clinical instruments. Many of today's instruments focus on detecting changes in anatomical structures, such as the nerve fiber layer. Our device, which is based on a modified fundus camera, seeks to detect changes in optical signals that reflect functional changes in the retina. The functional imager uses a patterned stimulus at wavelength of 535nm. An intrinsic functional signal is collected at a near infrared wavelength.

Measured changes in reflectance in response to the visual stimulus are on the order of 0.1% to 1% of the total reflected intensity level, which makes the functional signal difficult to detect by standard methods because it is masked by other physiological signals and by imaging system noise. In this paper, we analyze the video sequences from a set of 60 experiments with different patterned stimuli from cats. Using a set of statistical techniques known as Independent Component Analysis (ICA), we estimate the signals present in the videos. Through controlled simulation experiments, we quantify the limits of signal strength in order to detect the physiological signal of interest.

The results of the analysis show that, in principle, signal levels of 0.1% (-30dB) can be detected. The study found that in 86% of the animal experiments the patterned stimuli effects on the retina can be detected and extracted. The analysis of the different responses extracted from the videos can give an insight of the functional processes present during the stimulation of the retina.

1. INTRODUCTION

In the field of ophthalmology, visual field testing (perimetry) is the gold standard for detection and monitoring progression of diseases such as glaucoma. Perimetry is a functional test of the patient's vision, which is intended to detect defects on the visual field map. Unfortunately, perimetry remains a subjective test that requires the patient to make important judgments during the test that can be clouded by anxiety, fatigue, or lack of concentration. Additionally, the sensitivity of this test is poor. Investigators have found that over fifty percent loss of ganglion cells is necessary to detect loss of function with perimetry [26]. This results in low sensitivity and poor repeatability is frequently observed in areas where anatomical damage is suspected.

As early as 1949, Hill and Keynes linked the activity of the nerve cells with changes in their optical properties [2]. In 1986, Grinvald et al. showed that changes in the optical properties of the tissue could be used to study the functional architecture of the cortex [3]. Villringer and Chance used near-infrared light to assess brain activity in humans through the skull non-invasively [4]. The authors have reported on an optical imaging device of retina function (OID-RF) that has been developed in an attempt to improve the objectiveness of the test and the sensitivity for detection of damage and change over time [1,19,20,24]. Kardon et al. reported the first device to directly image the retina to record changes in 700 nm light caused by retinal activation in response to a 535 nm stimulus [4].

The OID-RF measures the increase or decrease in retinal reflectance due to changes in retinal metabolism thought to be a result of blood oxygen uptake and capillary response due to neural activity resulting from visual stimulation of the photoreceptors in the human retina. The functional measurements are stored as optical recordings (videos). The reflectance measurements recorded in these videos are a mixture of the signal that reflects the neuronal activity (functional signal) and signals related to background unknown sources and noise. Measured changes in reflectance in response to the visual stimulus are on the order of 0.1% to 1.0% of the total reflected intensity level which makes the functional signal difficult to detect by standard methods since it is masked by the other signals that are present. Our goal

is to extract the functional signal from others signals present during the process of stimulation of the retina. Various approaches have been used to improve the signal-to-noise (SNR) characteristics of the functional signal, such as integrating several sets of measurements to improve the SNR. For humans, it is difficult to collect a large number of data sets requiring an hour or more of imaging. So, it is important to know what the limits of the SNR are that will still allow one to detect the functional signal. To find those limits, a numerical experiment using Independent Component Analysis (ICA) [5-9] has been devised that integrates experimental data from a cat's retina.

In recent years, ICA has been applied to many biological related problems such as electroencephalography (EEG) data analysis [10, 11] and electrocardiogram (ECG) data analysis [12]. Stetter et al. applied ICA techniques to isolate changes on the brain cortex of a macaque monkey due to visual stimulation [13, 14, 15]. The authors have applied ICA techniques [16-20] to isolate the changes produced in the retina due to visual stimulation. In this paper we demonstrate the application of ICA to a set of data collected with the OID-RF in order to extract the functional signal due to retinal stimulation. To achieve our goal a set of synthetic simulations were performed to asses the efficiency of some of the most popular ICA algorithms in our particular problem. The algorithms that prove more suited to the problem are then tested on data collected in cat experiments.

The paper is organized as follows: Section 2 contains a description of the optical imaging device and how the data was collected. Section 3 shows the methods used in the analysis of the synthetically-generated data and the live cat data. Section 4 describes the synthetic simulation methods used to validate the use of ICA in the data. Section 5 shows the results obtained by applying the ICA techniques in both synthetic and live cat data. Discussion of the results and conclusions are given in the last two sections.

2. MATERIALS AND DATA COLLECTION

A new device for imaging the retina, the Optical Imaging Device for Retinal Function (OID-RF) was developed by Kardon, et al. [1]. The OID-RF is a non-invasive imaging device that measures changes in the levels of oxygenated blood due to patterned stimuli applied to the subject's retina. The hypothesis is that a visual stimulus may cause the retina to alter its level of blood volume and the ratio of oxygenated hemoglobin (HbO) to deoxygenated hemoglobin (Hb). This has the effect of altering the spectral reflectance characteristics of the retina and in turn results in a change in the reflected intensity of the image in the stimulated area.

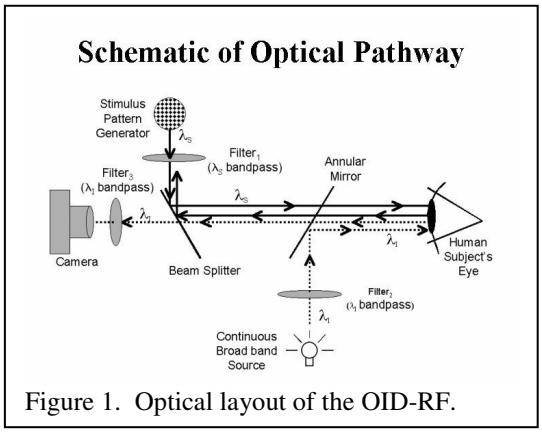

Figure 1. Optical layout of the OID-RF.

Figure 1 shows a diagram of how the OID-RF works. A constant interrogation light with wavelength in the red-near infrared wavelengths (780-850 nm) is projected over the subject eye. Simultaneously, a stimulus pattern at a green wavelength (550nm) is presented. The stimulus is projected onto the subject's eye. The reflected energy from the eye is then filtered by the beam splitter, which only allows the interrogation light to pass to the CCD camera. Kardon et al. presented a detailed description of the system in [1].

The experimental data was collected from a live cat. A single experiment (epoch) consists of 20 frames of 144 by 192 pixels each, at a frame rate of 2 Hz for a total recording time of 10 sec. The stimulus paradigm consists of a checkered pattern with alternating polarity that is off for the first 3 s, representing the baseline (pre-stimulus), on for 5 s of stimulation, and 2 s of recovery (post-stimulus). The stimulus can be applied to a vertical or horizontal region in the shape of a bar. Figure 2a is an image of the pre-stimulated (baseline) retina as represented in the interrogation band (near infrared). Figure 2b shows a vertical bar stimulus with the corresponding measured reflectance of the infrared signal during the maximum functional response signal (about the 5^{th} second or 10^{th} frame). Figure 2c presents the time plot of the functional response for the stimulated region. The region selected is approximately at the second white checkered box from the top. To the right of the same box another region is sampled that shows a negative response just outside the stimulated region.

The measured signals in Figure 2a and 2c form the basis of the numerical experiment and simulation. The baseline signal in Figure 2a allows one to estimate the spatial background signal from the pre-stimulated retina. This signal

contains physiological and device noise. The functional response signal in Figure 2c gives one a model of the reaction of the retinal to the stimulus. A positive or negative gain is applied to this functional response-based model to simulate an experiment with a human subject where the signal has been found to be substantially less than that of the cat. The numerical experiments are used to establish the detection limits using various signal processing techniques and also help define the experimental protocol for the human experiments, for example how many epochs or integration time are necessary to overcome the background noise.

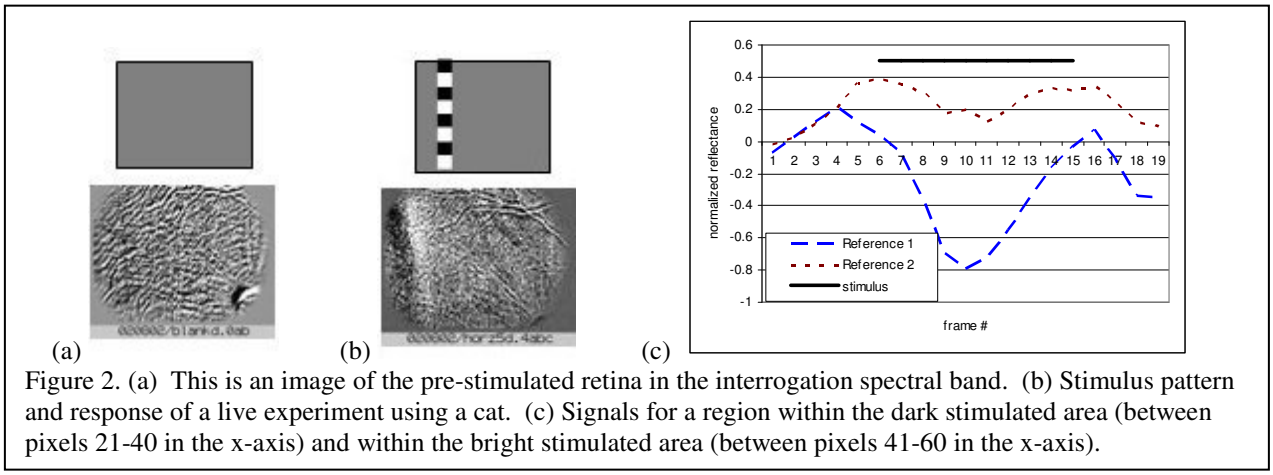

(a) (b) (c)

Figure 2. (a) This is an image of the pre-stimulated retina in the interrogation spectral band. (b) Stimulus pattern and response of a live experiment using a cat. (c) Signals for a region within the dark stimulated area (between pixels 21-40 in the x-axis) and within the bright stimulated area (between pixels 41-60 in the x-axis).

3. METHODS

This section describes the techniques used in the extraction of the signals resulting from the stimulation of the retina. As mentioned before, changes in reflectance due to visual stimulation of the retina are very small. It is our intention to apply ICA techniques to our data and to find out which of the algorithms is best suited for our experiments.

Let $X = [x_1(t)\, x_2(t) \ldots x_n(t)]$ be a set of observed random variables and assume that they come from the linear mixture of the components $S = [s_1(t)\, s_2(t) \ldots s_n(t)]$ by a mixing matrix A, as in

$$X = A\,S \qquad (1)$$

Then independent component analysis consists of estimating both A and S using only the observations X and the assumption that the source signals are statistically independent [21]. The statistical independence of the sources means that their joint probability can be factorized as

$$p(S) = \prod_{i=1}^{N} p(s_i) \qquad (2)$$

where $p(s_i)$ is the individual probability density function (pdf) of each of the sources and N is the number of sources.

For this study we selected 5 different ICA algorithms: Infomax; which uses maximum likelihood estimation (MLE) to extract the sources that give the highest probability for the observations; JADE a popular ICA algorithm that consists on using higher-order cumulant tensors; Fast-ICA that estimates the independent components by maximizing non-gaussianity; SOBI a method that incorporates time structure in the estimation of the sources; and ESD which is based on the same principles as SOBI but is optimized for image analysis. A brief description of how these algorithms work follows.

3.1. Infomax

The Infomax ICA algorithm was first proposed by Bell and Sejnowski [5] and is a generalization of the Infomax principle applied to ICA. The objective of the Infomax ICA algorithm is to reduce the redundancy between the sources. It is well known from information theory that when a set of signals are statistically independent, their mutual information is zero. As detailed in [22], the mutual information of the sources $I(S)$ is related to the joint entropy $H(g(S))$ of the sources passed through a set of nonlinear functions g_i, as in

$$I(S) = -H(g(S)) + E\left[\sum_i \log \frac{\left|g_i'(s_i)\right|}{p_i(s_i)}\right] \qquad (3)$$

Where $p_i(s_i)$ are the probability density functions (pdf) of the sources.

If the absolute values of the slopes of the sigmoid functions $\left|g_i'(s_i)\right|$ are the same as the independent components pdfs, $p_i(s_i)$, the Infomax (maximization of the joint entropy of the $g(S)$ vector) is the same as ICA (minimization of the mutual information).

Bell and Sejnowski derived a stochastic rule that maximizes the entropy of $g(S)$ using:

$$\Delta W \; \alpha \left(W^{-1}\right)^T + f(s)x^T \qquad (4)$$

Where W is the estimated inverse of the mixing matrix and vector function f has elements:

$$f_i(s_i) = \frac{\partial}{\partial s_i} \ln g_i'(s_i). \qquad (5)$$

When $g_i'(s_i) = p_i(s_i)$, the ICA algorithm is exact. Of course this leaves the problem that we need to know the pdf of the sources, which in most of the cases is unknown, but a rough approximation of the pdf is sufficient. For a more through discussion of how this affects the Infomax algorithm refer to [5, 22].

3.2. JADE

The Joint Approximate Diagonalization of Eigenmatrices (JADE) algorithm was proposed by Cardoso and Souloumiac in [23] and is based on the joint orthogonalization of the cumulant tensors. The cumulant tensor is defined as a four-dimensional array whose entries are given by the fourth order cross-cumulants of the data as in:

$$Q_x = \left\{cum\left(x_i, x_j, x_k, x_l\right) | 1 \le i, j, k, l \le n\right\}. \qquad (6)$$

The cumulant matrix $F_{ij}(M)$ associated with any $n \times n$ matrix M (later assumed to be an eigenmatrix) is defined as:

$$F_{ij}(M) = \sum_{kl} m_{kl} cum(x_i, x_j, x_k, x_l), \qquad (7)$$

where m_{kl} are the elements of the matrix M. We work with the case that the data follows the ICA model with whitened data

$$x = VAs = W^T s, \qquad (8)$$

where the whitened matrix is denoted by W^T. Eigenvalue decomposition (EVD) can be viewed as a diagonalization, when the JADE algorithm takes a set of matrices M_i, $i=1,\ldots,m$, and estimates the matrices $C=WF(M_i)W$ as diagonal as possible. The contrast function to measure the diagonality of the matrix C is:

$$\phi_{JADE}(W) = \sum_i \left\| diag\left(WF(M_i)W^T\right)\right\|^2 \qquad (9)$$

After some manipulations [23], the contrast function can be expressed as:

$$\phi_{JADE}(W) = \sum_{i,j,k,l=1,\ldots,n} \left| cum\left(y_i, y_j, y_k, y_l\right)\right|^2 \qquad (10)$$

where $y_i = Wx_i$. Maximization of ϕ_{JADE} is one method of joint diagonalization of $F(M_i)$.

3.3. Fast-ICA

The Fast-ICA algorithm was developed by Hyvarinen and Oja in [9] and is based on the minimization of gaussianity based on the *negentropy* concept. To define negentropy, we use the concept of differential entropy, defined as:

$$S(p_x) = -\int p_x(u) \log p_x(u)\, du, \qquad (11)$$

where S is the differential entropy of the random vector X with probability density function p_x. Then, the negentropy is defined as:

$$J(p_x) = S(\phi_x) - S(p_x), \qquad (12)$$

where ϕ_x is the gaussian density with the same mean and variance as p_x. The Fast-ICA algorithm then uses a fixed point algorithm to maximize negentropy.

The algorithm then computes the demixing matrix W in an iterative fashion, computing one row at a time using

$$w_i(j+1) = E\left(y\left(w_i^T(j)y\right)^3\right) - 3w_i(j), \qquad (13)$$

where $w_i(j+1)$ is the i-th row for the (j+1)-th iteration and y is the whitened version of the data.

3.4. SOBI

Our data set contains a temporal structure given by the stimulus and the sinusoids. When the independent components are time signals, they may contain much more structure than simple random variables. Some algorithms, like SOBI and ESD try to take advantage of the temporal structure of the data.

A form of the time structure is given by the time-lagged covariance matrix,

$$C_\tau^x = E\left\{x(t)\, x(t-\tau)^T\right\} \qquad (14)$$

When $\tau = 0$ we have the zero-lagged covariance matrix, which only contains second-order information and it is not sufficient for estimating the independent components. Since the sources are assumed to be statistically independent, we know that the lagged covariances are also zero. Thus, we need to estimate a matrix B such that the covariance of $y(t) = B\,x(t)$ satisfy [21]:

$$E\left\{y_i(t)\, y_j(t-\tau)^T\right\} = 0 \quad \forall i, j, \tau, i \neq j \qquad (15)$$

Based on this principle, the AMUSE algorithm [7] was developed. This algorithm is simple and fast to compute but it only works if all the eigenvalues of the time-lagged correlation matrix are different. An extension of the AMUSE algorithm considers different time lags τ instead of just one. The idea is to simultaneously diagonalize all the lagged covariance matrices. A way of measuring the diagonality of a matrix M is to use the operator

$$off(M) = \sum_{i \neq j} m_{ij}^2 \qquad (16)$$

which gives the sum of the squares of the off-diagonal elements of M. What we want is to minimize the sum of the off-diagonal elements of several lagged covariances. For this we use the whitening matrix W and the symmetric version $\bar{C}_\tau^y$ of the lagged covariance matrix. Denoting by S the set of lags τ, we can write the objective function:

$$J(W) = \sum_{\tau \in S} off\left(W \bar{C}_\tau^y W^T\right). \qquad (17)$$

Minimizing J under the constraint that W is orthogonal gives us the estimation method. The second-order blind identification (SOBI) algorithm [8] is based on this principle.

3.5. Extended Spatial Decorrelation

The extended spatial decorrelation (ESD) algorithm was proposed by Schiessl et. al. [14] and is an extension of the AMUSE algorithm (described in the previous section) for two dimensional spatial structures. It has been applied to brain imaging experiments [15] similar to the experiments set up in this paper.

4. SYNTHETIC SIMULATIONS

Since the amplitude of the reflected signal due to the functional response has been measured to be on the order of 0.1 to 1% of the total reflected infrared interrogation light, we design a series of experiments to quantify the performance of ICA algorithms in recovering the functional signal. The simulated videos are generated from a live cat experiment where no stimulus was applied, referred to as the baseline video. The data from the live cat experiments were provided by T'so [25]. This baseline video is altered by adding a synthetically generated functional response that is based on the model of an actual response shown in Figure 2c. A single video frame during the peak of the functional response in a live cat experiment is shown in Figure 3a. The resulting frames have similar spatial characteristics. Using the baseline video, the model of the functional response is applied. The result is presented in Figure 3b. This process allows one to produce videos by varying the amplitude in the functional signal and theoretically test the limits of each of the ICA algorithms. Presenting a realistic, but precisely known functional signal, also allows one to verify the performance by correlating the signal estimated by the algorithm with the known signal.

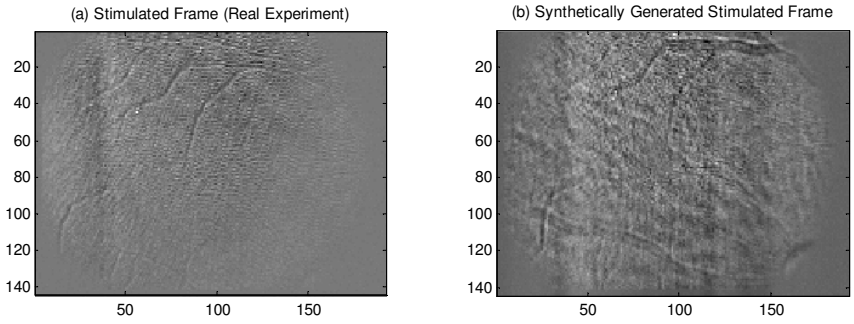

Figure 3: (a) Live cat frame from a stimulated cat retina. The vertical bar on the left is where the optical stimulation was applied. (b) Frame from the synthetically generated stimulated video.

The amplitude of stimulus applied to the baseline video is defined by its Stimulus-to-Background Ratio (SBR). The SBR is given as,

$$SBR(dB) = 10\log_{10}\frac{\sigma_S^2}{\sigma_B^2} \qquad (18)$$

Where σ_S^2 is the variance of the functional signal and σ_B^2 is the variance of the background.

Five videos were produced starting with the modeled functional signal and background from 0 dB to -40 db at -10 dB intervals. Note that the more negative the SBR value, the lower the amplitude of the functional signal. A 0 dB SBR indicates that the variance of the functional signal is equal to the variance of the video. A -30 dB SBR means that the variance of the functional signal is 0.1% of the variance of the video. Each video is processed by the five ICA algorithms, which estimated the sources and the mixing matrix; with the estimated sources yielding the spatial distribution of the functional response and the estimated mixing matrix giving us the time response of the corresponding estimated sources. The resulting extracted signals were then correlated with the model signal that was used to produce the video, i.e. ground truth. The correlation was used as the metric for comparison of the ICA algorithms. To understand the nature of the estimated signals, we re-write equation (1) with the actual dimensions of experimental data. The ICA model is now defined as:

$$X_{20\times 27648} = \hat{A}_{20\times 3}\,\hat{S}_{3\times 27648} \qquad (19)$$

Where the dimensions of the observations X correspond to 20 frames (images) of 144 by 192 pixels each (27648 total pixels). We arbitrarily choose the number of estimated sources to be three, since we are interested in finding 2 temporal responses and need an extra one to represent any other process. Therefore, the estimated mixing matrix $\hat{A}$ will have 3 column vectors of 20 points each, which will represent the time courses of the independent components. The estimated sources matrix $\hat{S}$ is composed of three row vectors, each of which will generate a 144 by 192 pixels image. These images are the ones that will give us the spatial distribution of the functional response.

Specifically, the results of the ICA algorithms were compared in the temporal and spatial domains. For the spatial domain, we correlated the sources as estimated by the ICA algorithm with a "reference frame," which is an image artificially generated by using a frame of pre-stimulated retina and the artificial stimulus on top, as seen in figure 4. For the temporal comparison, each row of the estimated mixing matrix, $\hat{A}$, was correlated with the modeled functional responses shown previously in Figure 2c. A high correlation means that the estimated mixing matrix is following the time trace of the functional response expected due to visual stimulation.

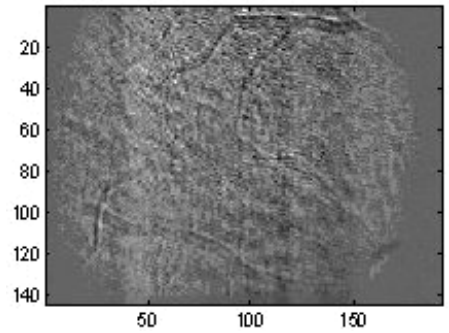

Figure 4: Spatial reference frame. The vertical stripe on the left (before marker 50 in the horizontal axis) is where the stimulus is applied.

5. RESULTS

5.1 Synthetic Stimulus Simulation

The ICA algorithms estimated the spatial/temporal signal with three components or sources. This was an arbitrary choice. Because one does not know a priori which component represents the functional signal, each component was correlated with the reference frame. In other words, to determine if the algorithms estimate the sources correctly, we need to correlate each column vector of the mixing matrix with the temporal references and each row of the sources with the spatial reference and then pick the highest correlation values obtained. Figure 5 shows the maximum absolute correlation values at zero lag. From this plot we see that the Infomax algorithm obtains correlation values above 0.8. Meanwhile, Jade, SOBI and ESD have correlation values between 0.6 and 0.9. Fast-ICA has the lowest correlations, ranging between 0.4 and 0.6. In most of the cases, a decrease of 10 to 20% in the correlation values is seen for SBR values less that -10dB.

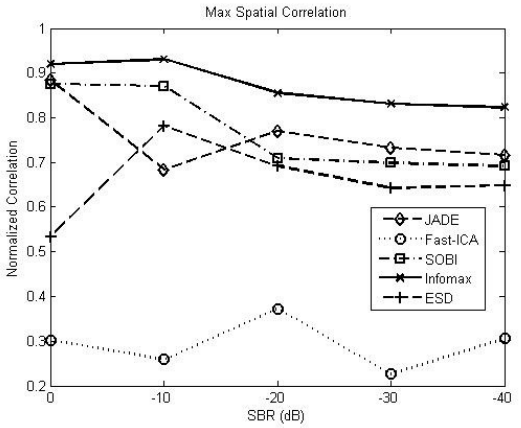

Figure 5: Spatial normalized correlations. Infomax has the highest correlations, all above 0.8. JADE, SOBI and ESD achieve correlation values around 0.7, while Fast-ICA has poor correlation values at all levels.

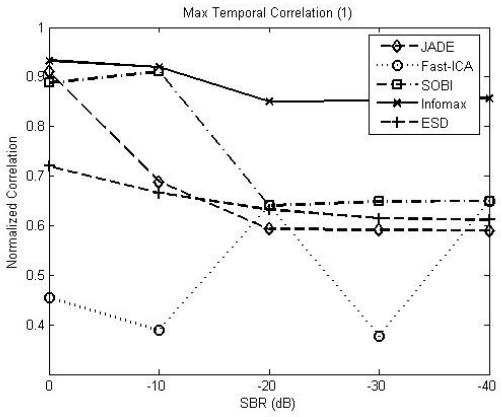

Figure 6: Temporal normalized correlations for the cat data with synthetic stimulus, correlated against reference signal 1. Infomax clearly outperforms the rest of the ICA algorithms.

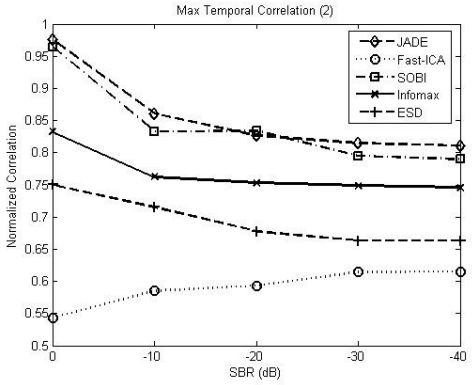

Figure 7: Temporal normalized correlations for the real data with synthetic stimulus, correlated against reference 2. JADE and SOBI have the highest correlation, with Infomax having slightly worse values.

The rows of the estimated mixing matrix were correlated to two reference signals. Figure 6 shows the results of the correlation with temporal reference 1, and here we see that Infomax reaches correlations above 0.9 for -10dB or more and above 0.85 for SBR values between -20 and -40dB. JADE and SOBI have similar results and show a sharp decrease in the correlation values for SBR values of -20dB or less. ESD correlation values remain mostly constant around 0.7, and Fast-ICA has inconsistent results ranging between 0.4 and 0.6.

The correlation values resulting from the correlation of the rows of the estimated mixing matrix and the temporal reference 2 are shown in figure 7. In this case, JADE and SOBI are the algorithms that obtain the highest correlations, with values above 0.8. Infomax correlation values are above 0.75, while ESD values are around 0.7. Fast-ICA results again have the lowest correlations, with values below 0.6.

5.2 Cat Experimental Results

Using the results of the synthetic simulations we narrowed the number of ICA algorithms to use with the cat data recordings to three: JADE, Infomax and SOBI. A total of 60 cat data experiments were processed, of which 18 had a vertical stimulus (Fig. 8a), 18 a horizontal stimulus (Fig. 8b), 3 a spot stimulus (Fig. 8c), 3 a full field stimulus and 18 were unstimulated (fig. 8d). We were able to visually identify 36 out of the 42 stimulated videos (86%).

Figures 9, 10 and 11 show a comparison of how the three algorithms extract the stimulus signal spatially and temporally for three different types of stimulation. Figures 9a to 9c show how the ICA algorithms locate the functional response to the vertical stimulus. Figure 9d show the timelines of these estimated components, as given by the estimated mixing matrices. Note how all three algorithms show a decrease in the reflectance when the stimulus is applied and the negative response peaks after 2 to 2.5 seconds of stimulation (frames 10 or 11). After reaching this negative peak the reflectance starts to increase again, surpassing the normal levels of reflectance, to finally go back to its original level when the stimulus is turned back off.

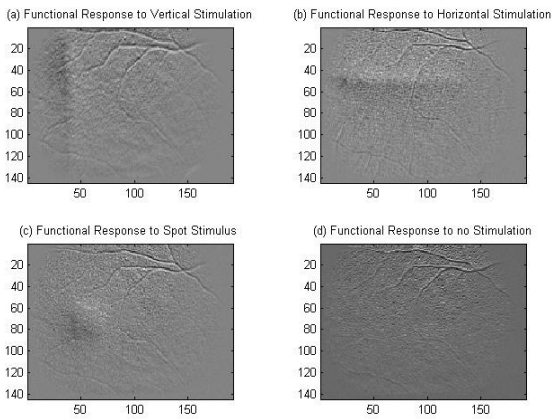

Figure 8. Different functional responses to Stimulation. (a) Response to vertical stimulus. (b) Response to horizontal stimulus. (c) Response to spot stimulus. (d) response when no stimulus is applied.

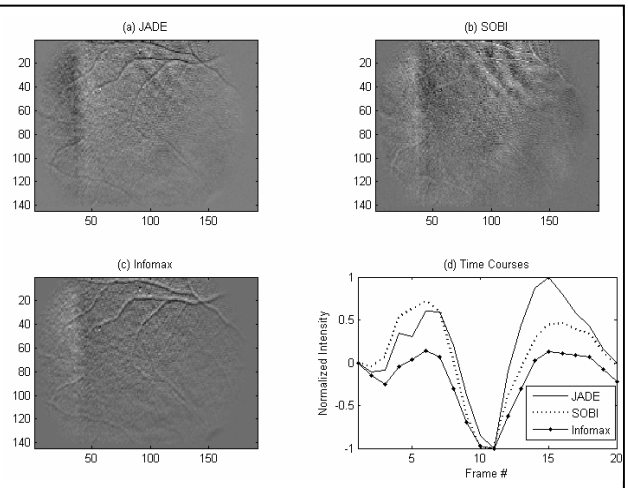

Figure 9: (a-c) Estimated spatial vertical functional signal extracted using JADE, SOBI and Infomax. (d) Estimated time courses for vertical stimulation.

The functional response for horizontal stimulation is similar to the one for vertical stimulation, as shown in figure 10. all the ICA algorithms estimate the spatial location of the functional response and as figure 10d shows, the timelines are similar but with a slight delay (1 frame) if compared to the response for the vertical stimulus. The response to the spot stimulus (figure 11) is similar to the ones in the two previous cases.

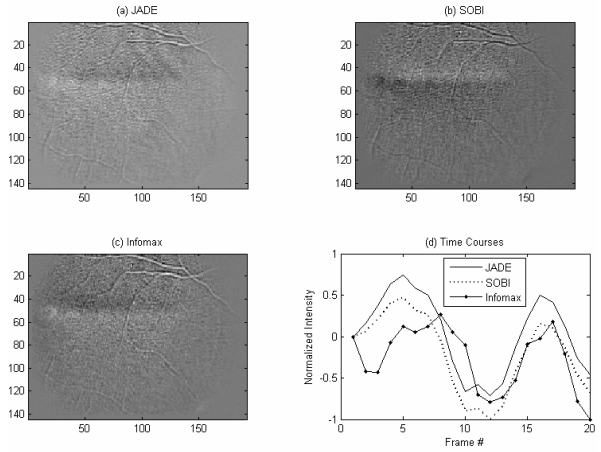

Figure 10: (a)-(c) Estimated spatial horizontal functional signal extracted using JADE, SOBI and Infomax. (d) Estimated time courses for horizontal stimulation.

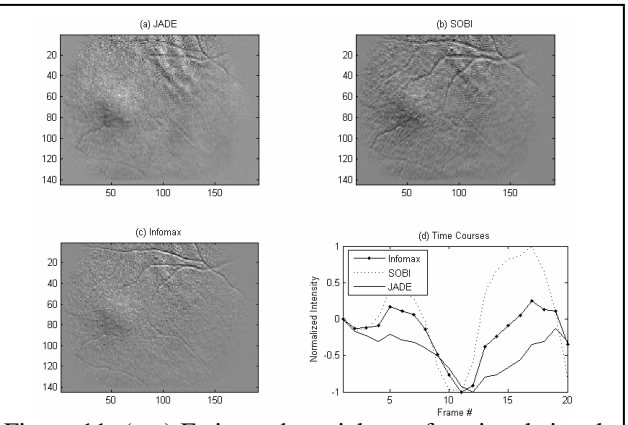

Figure 11: (a-c) Estimated spatial spot functional signal extracted using JADE, SOBI and Infomax. (d) Estimated time courses for spot stimulation.

6. DISCUSSION

The synthetic stimulus simulations have provided a means to analyze the feasibility of extracting a low amplitude functional signal in noisy reflectance images. The results of the spatial correlation of the estimated sources with the reference frame (Figure 5) showed that the Infomax algorithm achieves the highest correlation values. Infomax always provided an accurate location of where the visual stimulus had been applied. JADE and SOBI also produce good

correlation results, but not as high as Infomax. The results for these two algorithms allow us to locate the functional response. ESD produces marginal results, especially at the 0 dB SBR level, which is unexpected given the fact that at this level the stimulus is quite high. Fast-ICA produces poor results for the spatial reconstruction of the functional response.

The temporal correlations show how close the algorithms estimate the functional in the "dark" and "bright" regions where the functional response is located. The functional responses for these two regions are slightly different, with the dark region peaking negatively very fast and the bright region increasing its reflectance for about one second to then show a decrease in reflectance similar to the one in the dark region. The correlations results shown in Figure 6 show that Infomax is the algorithm that achieves the best results for the reference signal taken from the dark region. For SBR levels higher than -10 dB, JADE and SOBI achieve also high correlation values, but then those values sharply decrease when the SBR is lower than -20 dB. In contrast, when we compare the results of the reconstruction of the bright region of functional response, SOBI and JADE outperform Infomax, although not by much. We can hypothesize that SOBI performs better in this case because the reference signal has a more deterministic time structure, and since SOBI takes advantage of the time structure of the components it achieves those high correlation values. It is unclear why JADE performs better in this case, but we have observed that JADE is very consistent on the correlation values obtained, consistently having high enough values for detection of the functional signals. In the temporal experiment we again noted marginal performance by ESD and poor performance by Fast-ICA, which might be due to poor convergence for these specific types of signals or because of the dimensionality of the problem.

When analyzing the cat data recordings we noted several interesting results. First, it is clear how, as a result of the stimulation, two adjacent regions of contrasting reflectance are created. In the case of the vertical stimulation, the dark region is left to the bright region. When there is horizontal stimulation, the bright region is on top of the dark region, and most interesting, when there is a spot stimulation (small square) the left/bottom part of the square (lower triangle) forms the dark region and the right/upper part of the square (upper triangle) forms the bright region, as if the responses of the vertical and horizontal stimulation would have additive property. The nature of these phenomena is unknown to us, but several theories can be formulated . Another interesting result is the way the functional response changes the reflectance through time. At first when the stimulus is applied (frame 6) there is a slight increase in reflectance but then immediately it starts to decrease, to reach its negative peak between frames 10 to 12 (2 to 3 seconds after the start of stimulation). After this negative peak the signal goes back up to higher levels than the original ones to finally come back to the original state after the stimulus is turned off. These results are consistent with other hemodynamical processes observed in the brain using techniques such as functional magnetic resonance imaging (fMRI) and functional near infrared imaging (fNIR), which suggests that the same quantitative analysis carried out in this work could be applied to those problems.

Finally, when comparing the results obtained by the three different algorithms selected for the analysis of the cat recordings, we note that the three obtain similar estimated signals. If the reader notes a discrepancy in the bright/dark regions (as seen in figures 9b and 9c, for example) is because of the ambiguity problem inherent to ICA; in those cases the algorithms are estimating signals that are the negative of the real functional signals. This should not be a critical problem since we know how the spatial regions are supposed to be distributed. The resulting estimated images also show that SOBI generates slightly sharper edges on the stimulated region, especially in the vertical stimulation example.

7. CONCLUSSIONS

The experiments preformed by applying a synthetically generated functional response on top of an image of an unstimulated cat retina have provided us with information of the limits of detection achievable by the ICA algorithms. Our goal was to detect functional responses on the order of 0.1% (-30dB) of the total reflected signal. Our results show how three ICA algorithms; JADE, Infomax and SOBI produce estimates of the functional signals that are highly correlated with our references. This study will be more useful when analyzing data providing from human experiments, since in the human case the functional response is much more faint than in the cat; because of more noise sources such as movement (the cat is anesthesized during the experiments, the human is not), lack of focus (the human subject cannot withstand long periods of stimulation) and the complexity of the human retina.

The analysis of the cat data recordings corroborate the findings of the synthetic simulations, and also shows some interesting results such as the generation of a dark/bright contrasting region where the retina is stimulated and a time response that follows the same pattern as very well know neurophysiological processes studied with fMRI.

The 86% ratio of detection of the functional response could have been higher, but due to problems is alignment between the stimulus and the cat eye, in some cases the stimulus was applied outside of the field of view, producing no response.

In conclusion, the OID-RF has been demonstrated to produce a functional response in the cat retina due to visual stimulation. The analysis of the synthetic experiments has given us useful information in determining the threshold of stimulation that can be detected using the ICA algorithms. The analysis of these experiments could also be applicable to any area where a spatiotemporal dependence of the data is presented.

It is our intention to apply the results of this study in data from human experiments obtained by a new prototype of the OID-RF device. The human data results will be reported by Abramoff et al. [24], but the ICA algorithms have not been tried in those experiments yet.

8. REFERENCES

1. Kardon, R., Kwon, Y.H., Truitt, P.W., Nemeth, S.C., T'so, D. and Soliz, P., "Optical imaging device of retinal function," *SPIE Photonics West*, 2002. San Jose, CA.
2. Hill, D.K. and Keynes, R.D. J. *Physiol., Lond.* 108, pp 278-281, 1949.
3. Grinvald, A., Lieke, E., Frostig, R.D., Gilbert, C.D. and Wiesel, T.N., "Functional architecture of cortex revealed by optical imaging of intrinsic signals," *Letters to nature*, vol. 324, pp 361-364, November 1986.
4. Villringer, A. and Chance, B., "Noninvasive optical spectroscopy and imaging of human brain function," *Trends in Neuroscience* 20, 435-442 (1997).
5. Bell, A.J. and Sejnowski, T.J., "An information-maximization approach to blind separation and blind deconvolution," *Neural Comput.*, vol 7, no. 6, pp. 1003-1034, 1995.
6. Cardoso, J., "Infomax and maximum likelihood for blind source separation," *IEEE Signal Processing Letters*, vol. 4, no. 4, April 1997.
7. Molgedey, L. and Schuster, H.G., "Separation of a mixture of independent signals using time delayed decorrelations," *Physical Review Letters*, vol. 72, no. 23, June 1994.
8. Belouchrani, A., Abed-Meraim, K., Cardoso, J., Moulines, E., "A blind source separation technique using second-order statistics," *IEEE Transactions on Signal Processing*, vol. 45, no. 2, February 1997.
9. Hyvarinen, A. and Oja, E., "A fast fixed point algorithm for independent component analysis," *Neural Comput.*, vol. 9, pp. 1483-1492, 1997.
10. Makeig, S., Bell, A.J., Jung, T.-P. and Sejnowski, T.J., "Independent component analysis of electroencephalographic data," in *Advances in Neural Information Processing Systems*, MIT Press, Cambridge MA, pp. 145-151, 1996.
11. Jung, T.-P., Humpries, C., Lee, T.-W., McKeown, M.J., Iragui, V., Makeig, S. and Sejnowski, T.J., "Removing electroencephalographic artifacts by blind source separation," *Psychophysiology*, vol. 37, pp. 163-178, 2000.
12. Choi, S., Cichocki, A. and Amari, S., "Fetal electrocardiogram data analysis via flexible independent component analysis," in *The 4-th Asia-Pacific Conference on Medical & Biological Engineering (APCMBE'99)*, Seoul, Korea, 1999.
13. Stetter, M., Schießl, I., Otto, T., Sengpiel, F., Hübener, M., Bonhoeffer, T. and Obermayer, K., "Principal Component Analysis and Blind Separation of Sources for Optical Imaging of Intrinsic Signals". *NeuroImage,* vol. 11, pp. 482-490, 2000.
14. Schiessl, I., Schoner, H., Stetter, M., Dima, A. and Obermayer, K. "Regularized second order source separation," in *Proceedings of the Second International Workshop on Independent Component Analysis and Blind Signal Separation*, Helsinki, Finland, Vol. 2, pp. 111-116, 2000.
15. Schiessl, I., Stetter, M., Mayhew, J.E. W., McLoughlin, N., Lund, J.S. and Obermayer, K. "Blind signal separation from optical imaging recordings with extended spatial decorrelation," *IEEE Transactions on Biomedical Engineering*, vol. 47: pp. 573-577, May 2000.
16. Barriga, E.S., Soliz, P. and Truitt, P.W., "Functional signal detection in retinal videos," in *The 45-th IEEE International Midwest Symposium on Circuits and Systems (MWSCAS-2002)*, Tulsa, Oklahoma, 2002.

17. Barriga, E.S., Truitt, P.W., Pattichis, M.S., T'so, D., Kwon, R.H., Kardon, R.H. and Soliz, P., "Blind source separation in retinal videos," in *The SPIE's International Symposium Medical Imaging 2003*, San Diego, California, 2003.
18. Barriga, E.S., T'so, D.Y., Pattichis, M.S. and Soliz, P., "Independent Component Analysis for Processing of Retinal Responses to Patterned Stimuli," in *The 25th IEEE Engineering in Medicine and Biology Society (EMBS) annual International Conference*, Cancun, Mexico, 2003.
19. Abramoff, M.D., Kwon, Y.H., T'so, D., Li, H., Barriga, E.S., Soliz, P. and Kardon, R.H., "A Spatial Truncation approach to the Analysis of Optical Imaging of the Retina in Humans and Cats," in *The IEEE International Symposium on Biomedical Imaging (ISBI): From Nano to Macro*, Arlington, Virginia, 2004.
20. Abramoff, M.D., Kardon, R.H., T'so, D., Soliz, P, Barriga, E.S., Li, H. and Kwon, Y.H., "Intrinsic Optical Imaging of the Retina in Awake Humans," in *The 2004 Association for Research in Vision and Ophtalmology Annual Meeting*, Fort Lauderdale, Florida, 2004.
21. Hyvarinen, A., Karhunen, J., Oja, E., "Independent component analysis", John Wiley, New York, 2001.
22. Jung, T., et. Al. "Imaging Brain Dynamics Using Independent Component Analysis", in *Proceedings of the IEEE*, vol. 89, No 7, July 2001.
23. J.-F. Cardoso and A. Souloumiac, "Blind beamforming for non Gaussian signals", in *IEE Proceedings-F*, 140(6):362-370, 1993.
24. M.D. Abramoff, Y. H. Kwon, D. Ts'o, P. Soliz, B. Zimmerman, J. Pokorny and R. Kardon, "Visual stimulus induced changes in human near-infrared fundus reflectance", to be published in *Investigative Ophthalmology & Visual Sciences (IOVS)*.
25. DY Ts'o, Y Kwon, R Kardon, P Soliz, H Li, M Abramoff, M Zarella, "Signal sources observed with intrinsic signal optical imaging of the retina," in *The 2004 Association for Research in Vision and Ophtalmology Annual Meeting*, Fort Lauderdale, Florida, 2004.
26. Quigley HA, Dunkelberger GR, Green WR. Retinal ganglion cell atrophy correlated with automated perimetry in human eyes with glaucoma. *Am J Ophthalmol.* 1989;107:453–464.